

8-19-2015

Effect of gap flow on the shallow wake of a sharp-edged bluff body –mean velocity fields

A.M Shinneeb
University of Windsor

R. Balachandar
University of Windsor

Follow this and additional works at: <http://scholar.uwindsor.ca/civilengpub>

 Part of the [Civil and Environmental Engineering Commons](#)

Recommended Citation

Shinneeb, A.M and Balachandar, R.. (2015). Effect of gap flow on the shallow wake of a sharp-edged bluff body –mean velocity fields. <http://scholar.uwindsor.ca/civilengpub/1>

This Article is brought to you for free and open access by the Department of Civil and Environmental Engineering at Scholarship at UWindsor. It has been accepted for inclusion in Civil and Environmental Engineering Publications by an authorized administrator of Scholarship at UWindsor. For more information, please contact scholarship@uwindsor.ca.



Effect of gap flow on the shallow wake of a sharp-edged bluff body – mean velocity fields

A.-M. Shinneeb and R. Balachandar

Department of Mechanical, Automotive, and Materials Engineering, University of Windsor, Windsor, Canada

ABSTRACT

This experimental study was carried out to investigate the turbulent shallow wake generated by a vertical sharp-edged flat plate suspended in a shallow channel flow with a gap near the bed. The objective of this study is to understand the effect of the gap flow on the wake by studying two different gap heights between the channel bed and the bottom edge of the bluff body. These two cases will be compared to the no-gap case which is considered as a reference case. The maximum flow velocity was 0.45 m/s and the Reynolds number based on the water depth was 45,000. Extensive measurements of the flow field in the vertical mid-plane and in the horizontal near-bed, mid-depth, and near-surface planes were made using particle image velocimetry. This paper is part of an extensive study to characterise the gap-flow effects and is primarily concerned with the mean velocity fields, while a companion paper discusses the turbulence characteristics. The size of the wake identified in the horizontal planes is found to vary in the three planes, where the gap flow enhances the entrainment in the near-wake region in the near-bed velocity field. The results also revealed that, if the gap flow is weak, it is engulfed by the recirculation zone formed just behind the bluff body whose axis is perpendicular to the vertical mid-plane. On the other hand, if the gap flow is relatively strong, it penetrates in the downstream direction and only a portion of it is diverted upward to feed the recirculation zone.

ARTICLE HISTORY

Received 16 March 2015
Accepted 19 August 2015

KEYWORDS

Shallow wake; bluff body;
turbulence; PIV; POD

1. Introduction

Turbulent wakes generated from two-dimensional bluff bodies have been extensively investigated in the past due to their various applications in engineering. The flow is characterised by the formation of large recirculation zones and periodic (or quasi-periodic) shedding of vortices. Among these wakes that are commonly encountered in nature is the shallow wake flow. Such flows are generally bounded by a bottom solid wall and a top free surface, generating a wake region that has characteristics different from the well-known two-dimensional wakes. In addition, the horizontal width of such shallow wakes is usually larger than the depth of flow. [1,2]

The behaviour of shallow wakes has been investigated by a number of researchers (e.g. [3–7]). Akilli and Rockwell [7] investigated the near wake of a circular cylinder in a

shallow flow by means of flow visualisation and particle image velocimetry (PIV). They reported mean velocity, vorticity, Reynolds stress, and streamline topology results at three vertical elevations: near the bed, mid-distance, and near the free surface. It was concluded that the vortex formation in the near-wake region is a highly three-dimensional process. Chen and Jirka [3] noted that the mechanism of vortex stretching does not affect eddies of sizes comparable to the depth of the flow. It was argued that the resulting wake will carry dual characteristics – the structures of scales greater than the water depth exhibit inverse cascade in the spectral analysis, which is an indication of the two-dimensional turbulence. On the other hand, the structures of scale smaller than the flow depth demonstrate the behaviour of three-dimensional turbulence. More recently, Arindam et al. [8] carried out PIV measurements in the wake of a sharp-edged bluff body immersed in a shallow channel flow on three horizontal planes (near the bed, mid-depth, and near the free surface) at a Reynolds number, based on the water depth, of 18,000. The results showed large differences in the size of the recirculation zones between the three horizontal planes. Analysis of the mean flow and vortical structure results revealed that the entrainment from the sides towards the wake vertical mid-plane occurs in the three horizontal planes, but with different rates, which was attributed to the formation and distribution of the vortices near the bed and the free surface.

Numerous experimental and computational studies have been carried out to understand the influence of wall proximity on the flow past long cylinders of different cross sections (e.g. circular, square, triangular, etc.). When a bluff body is placed near a plane wall, vortex shedding characteristics and thus transport phenomena in the wake are significantly affected by the presence of the nearby wall, [9] and in fact vortex shedding can be suppressed completely if the wall is close enough. Because of the influence of vortex shedding on characteristics such as drag and mixing, it is important to understand the influence of the gap height (h_g) between the wall and the body on the wake flow. [10,11] Examples of engineering applications of this type of flow are encountered frequently such as the airflow around solar panels and road vehicles, the cooling of electronic components, and the flow past pipelines near the ground or in a sea or river bed.

Many studies have been carried out with circular cylinders oriented horizontally such that the cylinder spans the test section and is placed above the bed to form a gap. Bearman and Zdravkovich [10] investigated the influence of gap height on the vortex shedding and the spectral behaviour of the wake as well as the pressure distribution on the wall and on the cylinder. The experiments were conducted at a Reynolds number of 5×10^4 , while the boundary layer thickness was 80% of the cylinder diameter. A critical gap height was determined such that the vortex shedding was suppressed below this critical value and becomes independent of the gap height above this value. The influence of the boundary layer thickness on the behaviour of the turbulent flow past a circular cylinder near a solid plane wall was investigated by Buresti and Lanciotti. [12] It was reported that the effect of the gap height is strong on the mean velocity and turbulence quantities. Grass et al. [13] and Taniguchi and Miyakoshi [14] reported that there is a correlation between the critical gap height and the boundary layer thickness. However, the values reported in the two studies are different. More recently, Wang and Tan [15] studied the effect of the gap height on the near-wake flow characteristics of a circular cylinder close to the wall using a PIV system by considering various gap heights. The results included the mean velocity and Reynolds stress quantities, as well as vortical structures. This study

confirmed the results of earlier studies about the effect of the gap height on the vortex shedding.

60 The effect of the gap height on the wake flow behind square cylinders near a plane wall has also been investigated by a number of researchers (e.g. [9,16–19]). Similar conclusions as that noticed in the flow past circular cylinders were reported in these studies, although the values of the critical gap height and other related parameters were different. On the other hand, the effect of gap flow on the wake of a flat plate is scarce in literature. Krampa-
65 Morlu and Balachandar [20,21] carried out LDV measurements in the wake of a flat plate suspended in a shallow channel flow with a gap height of 5 mm between the plate and the channel bed. The velocity profiles were measured at downstream locations along the water depth in the near- and intermediate-wake regions, and also at upstream locations. In addition, the velocity profiles were also measured in the transverse direction at two vertical elevations, one in the middle of the water depth, and the other one in the middle of
70 the gap opening. It was concluded that the flow through the gap resembles the characteristics of a wall jet. Moreover, the mean velocity and Reynolds shear stress profiles indicated fast recovery of the flow towards the upstream state in the near-wall region. However, the turbulence intensity and quadrant analysis results revealed that the flow was still
75 influenced by the disturbance generated by the bluff body, especially away from the wall region.

The present study is an experimental investigation of the interaction of a shallow wake with a gap flow generated by a simple bluff-body geometry. The importance of this research stems from our desire to gain a better understanding of the turbulence phenomena to
80 improve methods of prediction and allow better control/exploitation of the dynamic flow features in a variety of engineering applications. Consequently, the use of a global quantitative/visualisation tool such as PIV for investigating the turbulent wake flow is an attractive option in this effort. The present work then describes a turbulent wake generated by flows past a vertical sharp-edged flat plate suspended in a shallow channel flow to create a gap
85 near the bed. This configuration generates a wall-jet-like flow which would suppress the formation of the horseshoe vortex near the bed. Extensive PIV measurements were obtained in the developing wake region at a Reynolds number of 45,000 to quantify the interaction between the gap flow and the wake. The objective of this study is to understand the effect of the gap flow on the wake by studying two different gap heights between the channel bed
90 and the bottom edge of the bluff body. These two cases will be compared to the no-gap case which is considered as a reference case. Specifically, this paper is the first part of an extensive study to characterise the gap-flow effects by investigating the mean velocity field to unveil the basic structure of the shallow wake with gap flow.

2. Experimental apparatus

95 The present experiments were carried out in a recirculating open water channel of rectangular cross section. The dimensions of the channel are 9.5 m long, 1.2 m wide, and 0.6 m deep. The side walls and the bottom of the flume were made of Plexiglas to allow measurements of the flow field using the PIV. The mean free-stream velocity U_∞ of the channel flow was 0.45 m/s. The depth of the water H in the channel was controlled using a tail-gate and nominally maintained at 100 mm in the measurement region. The aspect ratio
100 of the channel flow is 12, which ensures negligible secondary currents. The corresponding

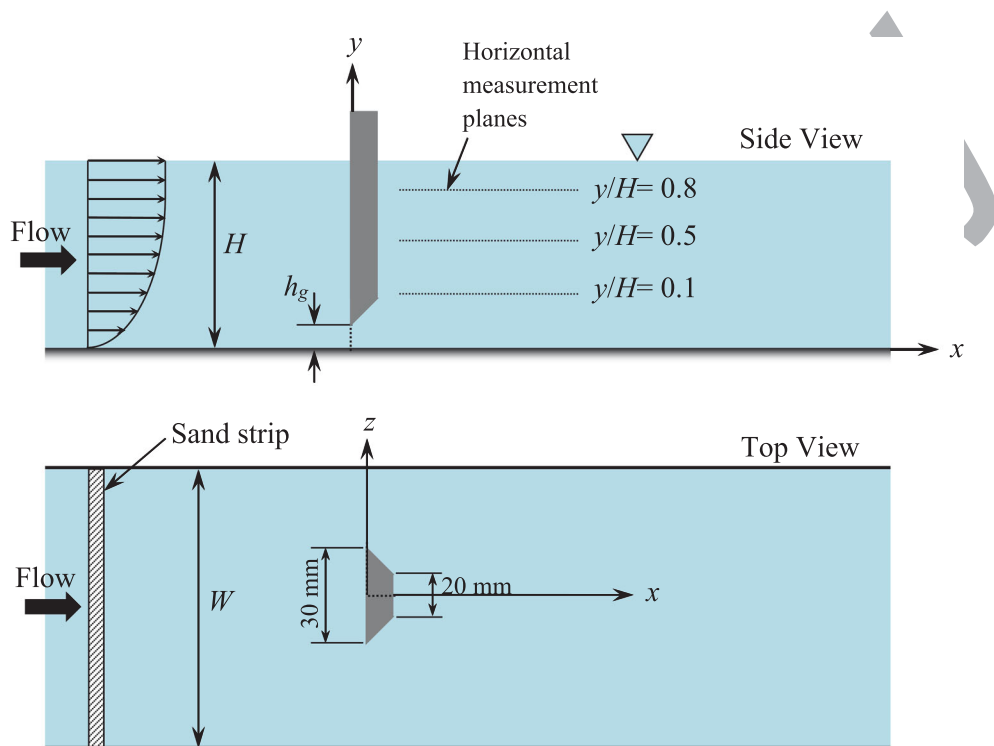


Figure 1. Schematic of the bluff body.

Reynolds number Re_H (based on the water depth H) was 45,000. A flow conditioner consisting of flow straighteners and wire screens was placed at the entrance of the channel to reduce turbulence. Measurements were performed at 4.9 m downstream of the flow conditioner. To ensure fully developed turbulent flow in the measurement area, the near-wall flow was tripped using a 25 mm wide sand strip spanning the entire channel width and was positioned at 3 m upstream of the measurement station.

The bluff body used in the present study was a sharp-edged flat plate 110 mm in height, 30 mm in width, and 6 mm in thickness, as shown in Figure 1(a) and 1(b). The bluff body was designed to have a flat shape on the upstream side, while it was chamfered at the edges on the downstream side. The body was inserted vertically in the channel flow, as shown in Figure 1, and supported by a steel bar from the top of the flume (not shown). Three positions of the bluff body were considered, one where the bluff body is in physical contact with the solid bed (no gap between the bluff body and the solid bed, gap height $h_g = 0$ mm), and two with gap heights h_g of 5 and 10 mm, respectively. The first case is known as the no-gap flow (NGF) case, while the others are known as the small-gap flow (SGF) and large-gap flow (LGF) cases. Care was taken to avoid streamwise vibrations of the bluff body. The horizontal confinement in the flume is negligible since the blockage ratio is only 2.5%. [22]

The origin of the coordinate system adopted in this study is located at the intersection of the vertical line of symmetry of the bluff body with the bed of the flume (see Figure 1).

The positive x -direction represents the distance measured along the channel flow starting from the origin at the upstream face of the bluff body and will be referred to as the streamwise direction, and the corresponding velocity component u is the mean streamwise velocity. The positive y -direction (measured upward from the bed of the flume) represents the vertical direction with a corresponding mean velocity component v . A right-hand rule was adopted for the coordinate system, and the z -direction was defined accordingly. The z -direction will be referred to as the transverse direction and the corresponding mean velocity is given by the symbol w .

3. PIV system and post-processing analysis










A TSI PIV system consisting of 120 mJ/pulse dual Nd:YAG lasers (New Wave Research) of 532-nm wavelength was employed in this study. The laser sheet was formed through a 500 mm or 1000 mm spherical lens and a -15 mm or -25 mm cylindrical lens depending on the desired size of the field of view (FOV). The resulting light sheet was approximately 2 mm thick in the area of interest.

Measurements will be reported on both vertical (x, y) and horizontal (x, z) planes that span streamwise locations in the range $0 < x/H < 3$. The vertical plane was positioned to cover the entire depth along the vertical mid-plane ($z/H = 0$). The horizontal planes were positioned at three elevations: near-bed ($y/H = 0.1$), mid-depth ($y/H = 0.5$), and near-free-surface ($y/H = 0.8$) planes. For each case, the velocity field was measured by taking three consecutive FOVs downstream of the bluff body. Table 1 summarises the case name, gap height, location, size, and spatial resolution of each FOV. The water in the flume was seeded with hollow-glass bead seed particles after filtering the water through a $5\text{-}\mu\text{m}$ filter. These particles have a specific gravity of 1.1 and a mean diameter of $10\text{ }\mu\text{m}$, yielding a Stokes settling velocity of 0.0054 mm/s . Therefore, these particles have the ability to faithfully follow the water flow (see Shinneeb [23] for more details).

The velocity fields were measured using a 2048×2048 pixels TSI PowerView Plus 4 MP camera and provides 12-bit output. At a framing rate of 1.04 Hz , 2000 image pairs were acquired at each location. A TSI PIV LaserPulse synchroniser was used to synchronise the operation of the camera with the laser. The camera was fitted with a 60-mm Micro-Nikkor or a $28\text{-}105\text{-mm}$ Zoom-Nikkor lens according to the object's distance, which was adjusted to give the required FOV. Image calibration was achieved by taking a picture of a steel ruler with 0.5-mm divisions. It was confirmed that there was negligible distortion over the FOV.

Image analysis was performed with correlation analysis INSIGHT 3G[®] software developed by TSI. The images were analysed with 32×32 interrogation areas using a fast Fourier transform (FFT) correlator. The interrogation areas were overlapped by 50%. The correlation peak was located within subpixel accuracy using a Gaussian curve fitting method. This analysis process yielded a final spatial resolution of 16 pixels. Table 1 summarises the size and the resulting spatial resolution of the velocity fields reported in this paper. Note that the *Distance from Bluff Body* column represents the streamwise distance from the bluff body to the left edge of the FOV. Following the correlation analysis, outliers were rejected using the cellular neural network method with a variable threshold technique, as proposed by Shinneeb et al. [24] The percentage of vectors rejected varied from 3% to 6% primarily at the edges of the velocity fields. Rejected vectors were replaced using a Gaussian-weighted mean of their neighbours.

Table 1. Summary of the velocity field characteristics.

h_g/H	Case name	Vertical position, y/H	Vertical (x, y) planes			Image size (mm × mm)	Spatial resolution (mm)
			Distance from bluff body				
			mm	x/H			
0.00	VSW001		− 1.99	− 0.020	70.5 × 70.5	0.55	
	VSW002		68.09	0.681	103.9 × 103.9	0.81	
	VSW003		167.34	0.167	103.6 × 103.6	0.81	
0.05	VSW051		− 1.99	− 0.020	70.5 × 70.5	0.55	
	VSW052		69.67	0.697	103.9 × 103.9	0.81	
	VSW053		167.34	0.167	103.6 × 103.6	0.81	
0.10	VSW101		− 1.99	− 0.020	70.5 × 70.5	0.55	
	VSW102		68.09	0.681	103.6 × 103.6	0.81	
	VSW103		167.34	0.167	103.6 × 103.6	0.81	
Horizontal (x, z) planes							
0.00	HSW001A	0.1	0.64	0.006	91.1 × 91.1	0.71	
	HSW002A	0.1	74.64	0.746	146.3 × 146.3	1.14	
	HSW003A	0.1	175.53	0.176	145.3 × 145.3	1.14	
0.05	HSW051A	0.1	0.64	0.006	91.1 × 91.1	0.71	
	HSW052A	0.1	74.64	0.075	146.3 × 146.3	1.14	
	HSW053A	0.1	175.53	0.176	145.3 × 145.3	1.14	
0.10	HSW101A	0.1	0.64	0.006	91.1 × 91.1	0.71	
	HSW102A	0.1	74.64	0.075	146.3 × 146.3	1.14	
	HSW103A	0.1	175.53	0.176	145.3 × 145.3	1.14	
0.00	HSW001B	0.5	− 1.88	− 0.019	101.4 × 101.4	0.79	
	HSW002B	0.5	67.10	0.671	157.0 × 157.0	1.23	
	HSW003B	0.5	171.45	0.171	153.4 × 153.4	1.20	
0.05	HSW051B	0.5	− 1.88	− 0.019	101.4 × 101.4	0.79	
	HSW052B	0.5	67.10	0.671	157.0 × 157.0	1.23	
	HSW053B	0.5	171.45	0.171	153.4 × 153.4	1.20	
0.10	HSW101B	0.5	− 1.88	− 0.019	101.4 × 101.4	0.79	
	HSW102B	0.5	67.10	0.671	157.0 × 157.0	1.23	
	HSW103B	0.5	171.45	0.171	153.4 × 153.4	1.20	
0.00	HSW001C	0.8	− 6.18	− 0.062	103.8 × 103.8	0.81	
	HSW002C	0.8	64.69	0.647	164.7 × 164.7	1.29	
	HSW003C	0.8	165.44	0.165	164.0 × 164.0	1.28	
0.05	HSW051C	0.8	− 6.18	− 0.062	103.8 × 103.8	0.81	
	HSW052C	0.8	64.69	0.647	164.7 × 164.7	1.29	
	HSW053C	0.8	165.44	0.165	164.0 × 164.0	1.28	
0.10	HSW101C	0.8	− 6.18	− 0.062	103.8 × 103.8	0.81	
	HSW102C	0.8	64.69	0.647	164.7 × 164.7	1.29	
	HSW103C	0.8	165.44	0.165	164.0 × 164.0	1.28	

4. Uncertainty analysis

The uncertainty of the PIV data is generally a function of the experimental settings (the flow conditions and image acquisition) and the image correlation analysis. [25] The error sources of the experimental conditions usually come from the instruments' calibration, image calibration, image distortion, etc., whereas the image correlation analysis is influenced by 170

particle image size, interrogation area size, particle seeding density, computational techniques, velocity gradients, and three-dimensional (out-of-plane) motion. In this study, the experiments were carried out carefully to reduce the uncertainty, and the maximum error in the velocity U_∞ at inlet is estimated to be 1.57%. Moreover, the error sources during the image acquisition can arise from the position and alignment of the calibration ruler compared to the laser sheet, as well as the accuracy of identifying pixel distance on the ruler-graduation image. The errors are estimated to be 0.5 mm, 2° , and 1 pixel, respectively (see the guideline of uncertainty analysis of PIV data-set proposed by the International Towing Tank Conference 2008 [26] for more details). Thus, the total uncertainty of the experimental conditions becomes 0.02%.

To quantify the uncertainty that comes from the image correlation algorithms, the analysis was performed by generating synthetic images with characteristics similar to the real images and known values of the particle displacements. As described in Bugg and Rezkallah,[27] the characteristics of the simulated images were quantified by the following parameters: background noise, number of paired and spurious particles, particle diameter, particle intensity, and displacement magnitude. These characteristics were obtained from the real images using MATLAB software. The simulated images were then analysed using the same procedures applied to the real images, and the outliers were detected and replaced using the same techniques as in the real data. Finally, both systematic and random uncertainties were determined by comparing the known and measured particle displacements. Thus, the relative uncertainty of the maximum displacement (8 pixels) of the instantaneous velocity fields is found to be about 1.43%. Including the error in the experimental settings, the relative error for the instantaneous velocity fields becomes 2.12%. Consequently, the relative error of the fluctuating velocity field increases by about one order of magnitude (see also Shinneeb [23] for similar analysis).

5. Results and discussions

The present paper investigates the effect of the gap flow on the mean flow field in the wake of a shallow smooth open channel flow at a Reynolds number Re_H of 45,000. Three cases of gap heights $h_g/H = 0, 0.05, \text{ and } 0.10$ of the bluff body are investigated, where the gap height $h_g/H = 0$ is called the NGE case and is used as a reference case. The other two cases ($h_g/H = 0.05$ and 0.10) are referred to as SGF and LGF.

5.1. Mean velocity profile of the approach flow

The purpose of this section is to document the boundary layer characteristics of the channel flow before inserting the bluff body. To confirm that the turbulent flow is fully developed, the velocity profiles in the measurement area were examined, which showed that the vertical distribution of the velocities remains almost unchanged in the downstream direction. In addition, a comparison between the approaching streamwise velocity u profile and well-documented channel flow results is made. The free-stream velocity U_∞ of the channel flow was 0.45 m/s. The boundary layer thickness δ perpendicular to the bed was estimated (based on $0.995U_\infty$) to occupy $\sim 82\%$ of the shallow water layer H . Similarly, the boundary layer thickness formed on the side walls is expected to be in the same order of magnitude as the one formed near the bed, which indicates that there is negligible influence of the side

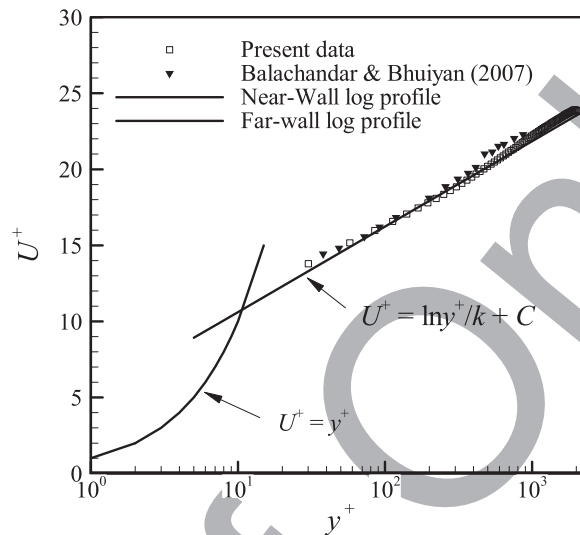


Figure 2. Mean streamwise velocity distribution of the smooth channel flow using inner and outer coordinates.

walls on the velocity field in the area of measurement. The displacement thickness δ^* and momentum thickness θ were estimated to be 11.6 and 7.8 mm, respectively. The resulting shape factor is 1.49 and the Reynolds number based on the momentum thickness Re_θ is 3524.

Figure 2 shows distribution of the streamwise component of the mean velocity in the channel flow in terms of the dimensionless wall velocity $U^+ (= u/u_\tau)$ and vertical axis $y^+ (= yu_\tau/\nu)$. The friction velocity u_τ , defined as $\sqrt{\tau/\rho}$, was determined by the Clauser chart method, [28] which is based on the assumption that the velocity profile follows a universal logarithmic form in the overlap region of the boundary layer. In this study, the friction velocity u_τ was estimated to be 19.2 mm/s. The corresponding skin friction coefficient C_f , defined by $2(u_\tau/U_\infty)^2$, was found to be 3.64×10^{-3} . The viscous length scale l_v , defined by (ν/u_τ) , where ν is the kinematic viscosity of the fluid) was estimated to be 0.052 mm. The present velocity profile was also compared with the experimental results of Balachandar and Bhuiyan [29] for smooth channel flow at a similar Reynolds number. The present results are in good agreement with the previous channel flow data.

5.2. Examples of instantaneous velocity fields of the wake flow

Selected examples of instantaneous velocity fields behind the bluff body are shown in **Figure 3**. This figure consists of three columns which show the velocity fields in three horizontal planes at (i) $y/H = 0.1$, (ii) $y/H = 0.5$, and (iii) $y/H = 0.8$. Each column consists of three plots (a, b, and c) which display the velocity fields at gap heights $h_g/H = 0, 0.05$, and 0.10, respectively. These plots are selected based on the clarity of the phenomena to be discussed, but they are uncorrelated. In this figure, the locations x and z are normalised by the water depth H . Note that the bluff body edges are at $z/D = \pm 0.15$. In these plots, only every third vector is shown in both directions.

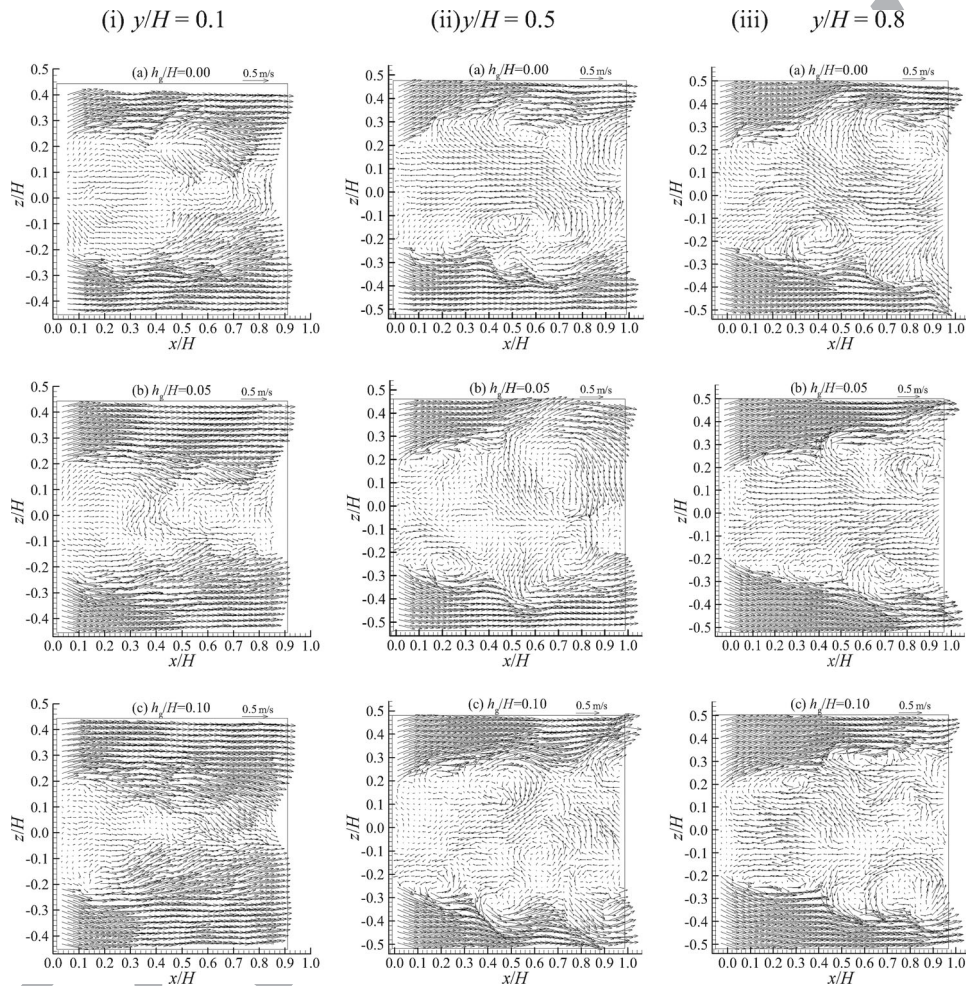


Figure 3. Examples of instantaneous velocity fields measured on the horizontal plane: (i) $y/H = 0.1$, (ii) $y/H = 0.5$, and (iii) $y/H = 0.8$. Each column (i, ii, and iii) consists of three plots (a, b, and c) which display the velocity fields for gap heights $h_g/H = 0, 0.05$, and 0.10 , respectively. Locations x and z are normalised by the water depth H .

From the first glimpse, the plots in [Figure 3](#) show that the size of the wake varies in the three planes where the smallest wake is seen in the near-bed plane ($y/H = 0.1$), and it becomes even smaller with increasing the gap flow. Another observation is the direction of flow in the three planes which appears different. Plots (a)–(c) in [Figure 3\(i\)](#) show that the flow is positive (forward) just behind the bluff body in the near-bed plane, while the flow is negative (backward) in the upper planes (see [Figure 3\(ii\)](#) and [3\(iii\)](#)). The plots also display the existence of clockwise (CW) and counter-clockwise (CCW) instantaneous swirling flow regions in most of the plots, particularly the mid-depth and near-surface planes, which appear to drive the flow in the wake region. However, such swirling flow regions are not seen for the LGF case ($h_g/H = 0.10$) in the near-bed plane (see plot (c) in [Figure 3\(i\)](#)). The reason is obviously because the position of this plane in this case coincides with the bottom edge of the bluff body, where the flow suppresses the formation of the swirling flow.

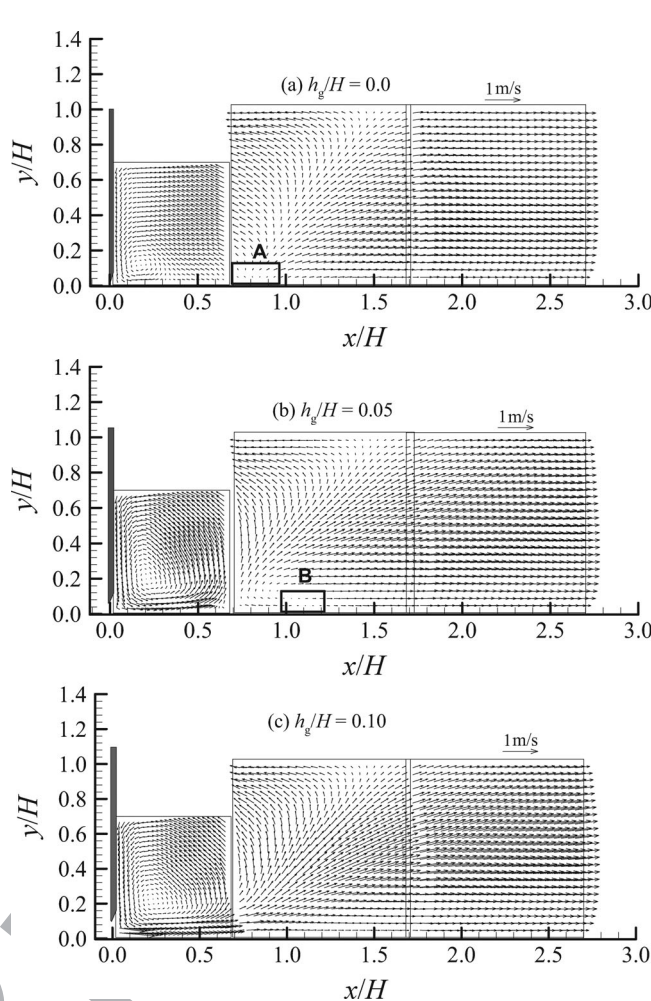


Figure 4. Mean velocity vector fields measured on the vertical mid-plane ($z/H = 0$) for (a) $h_g/H = 0$, (b) $h_g/H = 0.05$, and (c) $h_g/H = 0.10$.

The presence of the instantaneous swirling flow regions may be attributed to the formation of energetic vortical structures, which promote the formation of instantaneous swirling motion. More details about the effect of gap flow on the wake region are presented below. 250

5.3. Mean velocity fields of the wake flow

This section presents the mean velocity field of the shallow wake behind the bluff body on vertical and horizontal planes for gap heights $h_g/H = 0, 0.05$, and 0.10 . The size and spatial resolution of these FOVs are given in Table 1. The streamwise x -, vertical y -, and transverse z -axes are normalised by the water depth H . 255

Figure 4(a) displays the development of the velocity field in the downstream direction measured on the vertical plane ($z/H = 0$) for gap height $h_g/H = 0$. It can be seen that a relatively large recirculation zone is generated just behind the bluff body. The first FOV in

260 this figure, which displays only 70% of the water depth H , does not capture the whole size of the zone. The centre of the recirculation zone is located close to the flume bed at $x/H = 0.18$ and $y/H = 0.11$. At downstream locations, the velocity components (u and v) have positive and almost equal magnitudes along the diagonal of the second FOV. Furthermore, the flow to the left of the diagonal appears to return to feed the recirculation zone, while the flow
265 to the right of the diagonal moves in the downstream direction. This behaviour can also be seen in the gap-flow cases ($h_g/H = 0.05$ and 0.10) shown in Figure 4(b) and 4(c). However, there is a difference between the three cases in the position of the recirculation zone centres, where the horizontal x/H and vertical y/H positions are 0.21 and 0.20 for $h_g/H = 0.05$, and 0.24 and 0.21 for $h_g/H = 0.10$, respectively. It is clear that the increase in the gap flow causes
270 a shift of the recirculation centre upwards and to the right.

The effect of the gap flow on the wake velocity field is visualised in Figure 4 by comparing the SGF ($h_g/H = 0.05$) and LGF ($h_g/H = 0.10$) velocity fields with the NGF case ($h_g/H = 0$). In the NGF case (Figure 4(a)), it can be observed that an almost stagnant region (u and v are very small) close the bed (labelled A) is formed just behind the downstream boundary
275 of the CCW rotating recirculation zone in the range $x/H \approx 0.7-0.9$. At the boundary of this stagnant zone, the flow increases in all direction to form forward, upward, and backward flows. This behaviour suggests that there is a strong transverse entrainment (w component) in this region which is responsible for feeding the above-mentioned flows. Similarly, in the SGF case shown in Figure 4(b), a relatively stagnant region can also be seen approximately
280 in the same region (labelled B). In addition, the gap flow appears to be completely engulfed by the recirculation zone and directed upward before it reaches the stagnant zone. The reason is likely because the gap flow in this case (SGF) does not have enough momentum to overcome the influence of the recirculation field. Conversely, in the LGF case shown in Figure 4(c), there is no stagnant region and the gap flow is energetic enough to penetrate
285 in the downstream direction and also feed the upward flow.

To evaluate the effect of the gap flow on the velocity field in the horizontal planes, Figures 5-7 show the velocity fields at vertical elevations $y/H = 0.1, 0.5$, and 0.8 , respectively. Each figure consists of three plots (a-c) of the velocity field for gap heights $h_g/H = 0, 0.05$, and 0.10 , in the range $0 < x/H < 3$ are shown. From the first glimpse, the size of the
290 mean recirculation zones varies in the three planes as observed in the instantaneous velocity fields discussed in Section 5.2, where the streamwise length of the wake increases in the upper planes. The velocity field in the near-bed plane ($y/H = 0.1$) shown in Figure 5(a)-(c) displays the whole velocity field for the three gap heights. It can be seen that the flow is forward just behind the bluff body. Conversely, Figures 6 and 7 show that the flow is backward
295 in the same region. This can be clarified with the help of Figure 4, which shows that the vertical position of the near-bed plane ($y/H = 0.1$) is located below the centre of the CCW rotating recirculation zone, while the mid-depth ($y/H = 0.5$) and near-surface ($y/H = 0.8$) planes are located above the centre of the zone. Moreover, Figure 5 shows that the backward flow region decreases (and is finally eliminated) with increasing the gap height. However,
300 the effect of the gap flow seems to be qualitatively negligible at downstream locations. More detailed velocity profiles about the wake flow field will be presented in Section 5.6.

Another interesting feature that can be observed in most of the horizontal velocity fields is the presence of stagnant (or almost stagnant) region near the vertical mid-plane ($z/H = 0$). By inspecting Figure 4, this region corresponds to strong mean vertical velocity v component. For instance, the position of the almost stagnant region in the near-bed plane for

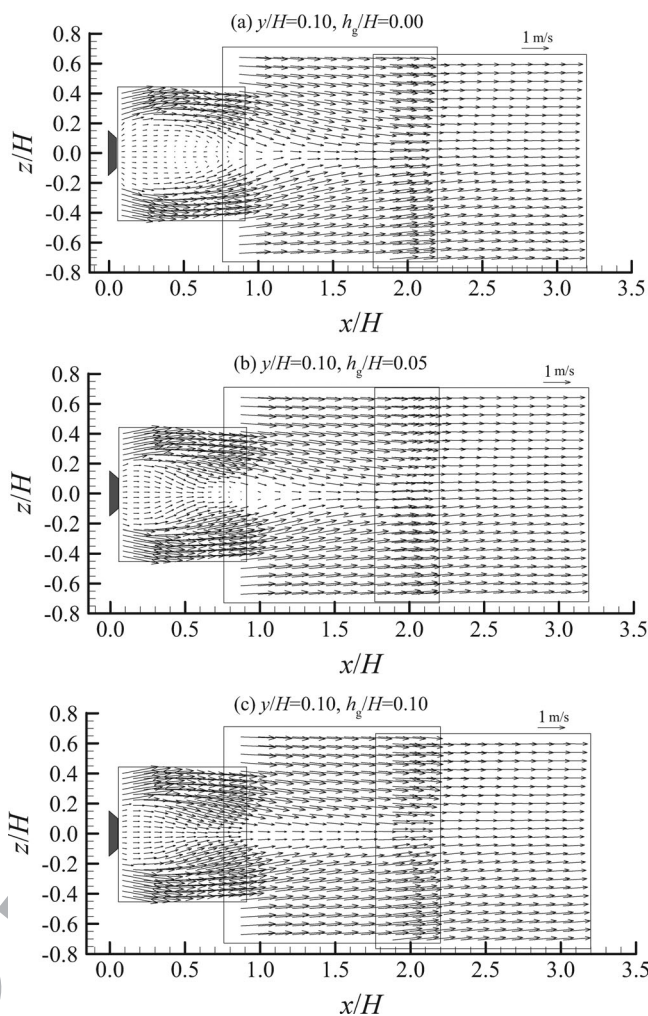


Figure 5. Mean velocity vector fields measured on the horizontal near-bed plane ($y/H = 0.1$) for (a) $h_g/H = 0$, (b) $h_g/H = 0.05$, and (c) $h_g/H = 0.10$.

the NGF and SGF cases, shown in [Figure 5\(a\)](#) and [5\(b\)](#), lies in the range $0.8 < x/H < 1.0$. It can be seen that the streamwise velocity u component becomes stronger to the right side of this region, compared to u in the left side. This indicates that a portion of the vertical flow contributes to the magnitude of u . Similarly, the position of the almost stagnant region in the mid-depth and near-surface velocity fields, shown in [Figures 6](#) and [7](#), lies in the range $1.0 < x/H < 1.2$ and $1.4 < x/H < 1.6$, respectively. According to [Figure 4](#), the backward and forward flows at the left and right sides of the stagnant regions, respectively, are fed by the vertical flow.

5.4. Variation of the mean central velocity with the streamwise distance

The variation of the mean central velocity in the vertical mid-plane ($z/D = 0$) of the wake (u_c) with the streamwise distance x is shown in [Figures 8](#) and [9](#). In these figures, the mean

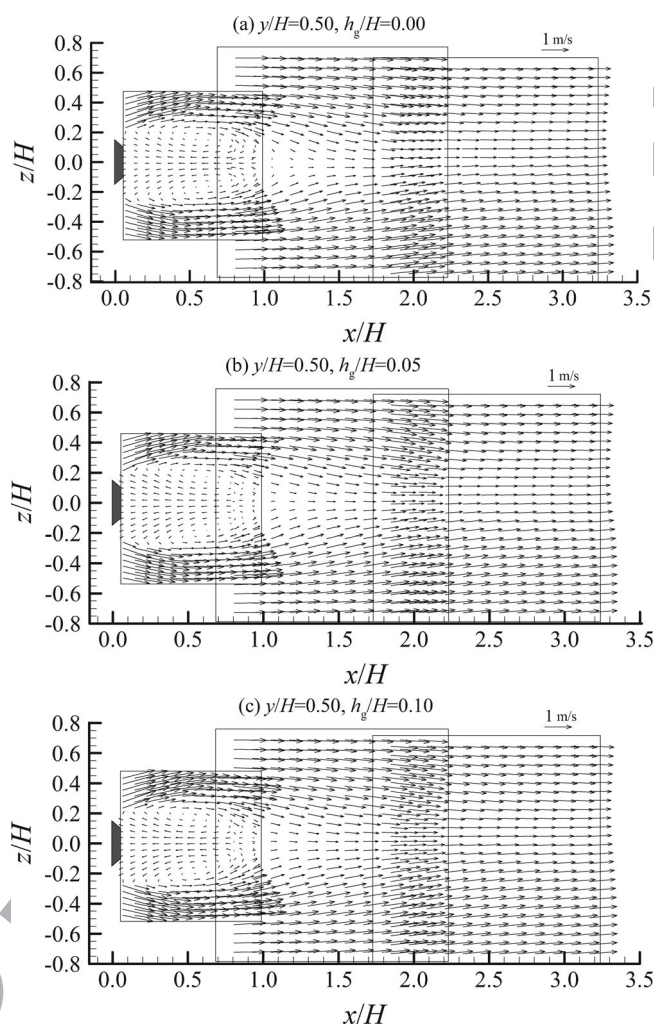


Figure 6. Mean velocity vector fields measured on the horizontal mid-depth plane ($y/H = 0.5$) for (a) $h_g/H = 0$, (b) $h_g/H = 0.05$, and (c) $h_g/H = 0.10$.

central velocity u_c is normalised by the mean streamwise velocity U_s ($U_s = 0.33$, 0.42 , and 0.445 m/s at the corresponding vertical location $y/H = 0.1$, 0.5 , and 0.8 , respectively) of the channel flow without the body, and the streamwise distance x is normalised by the water depth H . The mean central velocity u_c was obtained by fitting the horizontal profiles of the mean velocity defect $\Delta u (= u - U_s)$ with a Gaussian profile using Levenberg–Marquardt non-linear fitting algorithm. However, the defect velocity Δu in the first FOV was entered manually because the profiles are not Gaussian and cannot be fitted. The advantage of fitting is to extract the required information such as the central velocity u_c , the position of the central velocity z_c , and the position of the half-width $W_{0.5}$ from each profile simultaneously, and with a better accuracy since the noisy points are smoothened.

Figure 8(a)–(c) illustrates the difference between the three normalised central velocity u_c/U_s profiles in the three horizontal planes ($y/H = 0.1$, 0.5 , and 0.8 , respectively) at a specific gap height h_g/H . Figure 8(a) shows that the flow is forward (positive) just behind

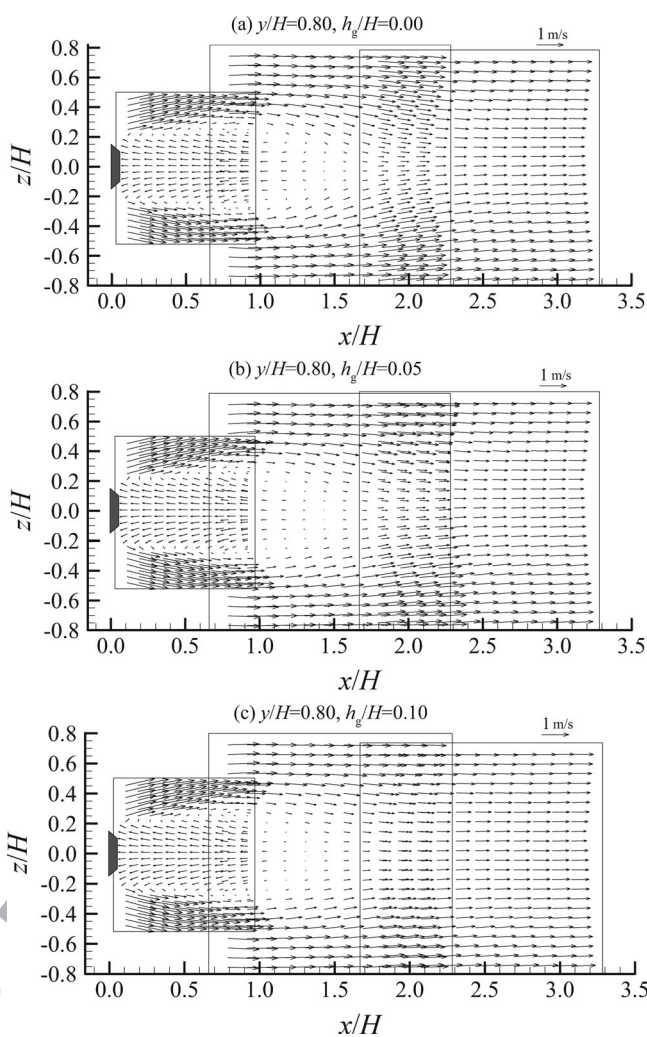


Figure 7. Mean velocity vector fields measured on the horizontal near-surface plane ($y/H = 0.8$) for (a) $h_g/H = 0$, (b) $h_g/H = 0.05$, and (c) $h_g/H = 0.10$.

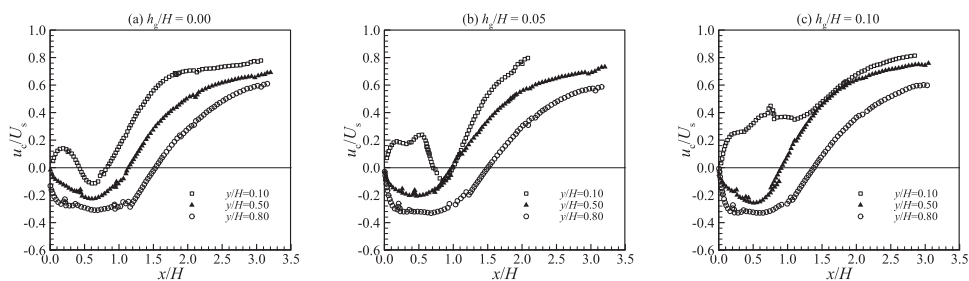


Figure 8. Variation of the mean streamwise central velocity u_c in the streamwise direction x extracted from the three horizontal planes for (a) $h_g/H = 0$, (b) $h_g/H = 0.05$, and (c) $h_g/H = 0.10$. Both u_c and x are normalised by U_s and H , respectively.

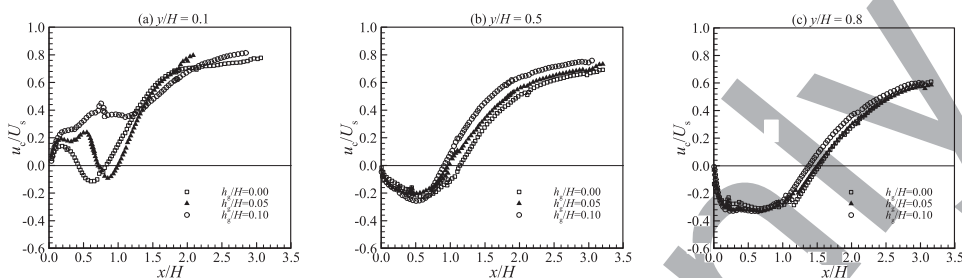


Figure 9. Variation of the mean streamwise central velocity u_c in the streamwise direction x for the three gap heights h_g/H at (a) $y/H = 0.1$, (b) $y/H = 0.5$, and (c) $y/H = 0.8$. Both u_c and x are normalised by U_s and H , respectively.

330 the bluff body in the near-bed plane ($y/H = 0.1$) for $h_g/H = 0$, becomes reverse flow
 (negative) from $x/H = 0.43$ to 0.83 , and then forward again after this point. According
 to [Figure 5\(a\)](#), the first stagnant point ($u_c = 0$) is a result of the forward and backward
 335 velocities which meet at that point, while the second stagnant point represents the loca-
 tion of the strong vertical flow ($+v$) which was split into three portions: one portion con-
 tinued upward ($+v$), the second portion supplied the reverse velocity ($-u$), and the third
 portion supplied the forward velocity ($+u$). As well, the curves in the mid-depth ($y/H =$
 0.5) and near-surface ($y/H = 0.8$) planes demonstrate the presence of a reverse flow, which
 appears to be relatively stronger in magnitude, particularly in the near-surface plane com-
 pared to the near-bed plane. According to this figure, the streamwise location where the
 340 central velocity u_c becomes zero is at $x/H \approx 1.14$ and 1.52 for $y/H = 0.5$ and 0.8 , respec-
 tively. These values are consistent with the stagnant regions in the horizontal planes dis-
 cussed in [Section 5.3](#). [Figure 8\(a\)](#) also illustrates that u_c/U_s varies linearly with x/H at a
 relatively high rate in the range $0.0 \leq x/H \leq 1.5$, $0.0 \leq x/H \leq 1.6$, and $1.3 \leq x/H \leq 1.8$ for
 $y/H = 0.1$, 0.5 , and 0.8 , respectively. Afterwards, u_c/U_s appears to vary at a much slower
 345 rate.

The central velocity u_c/U_s profiles for the SGF ($h_g/H = 0.05$) shown in [Figure 8\(b\)](#) resem-
 ble the corresponding profiles of the NGF case shown in [Figure 8\(a\)](#). However, the u_c/U_s
 profile in the near-bed plane ($y/H = 0.1$) shows that the length of the forward flow (just
 behind the bluff body) becomes larger because of the gap flow. In addition, the reverse flow
 350 in the near-bed plane appears to be slightly shifted downstream as a result of the SGF which
 seems to be not strong enough to overcome the reverse flow. Similar to the NGF case, the
 second stagnant point at $x/H \approx 0.99$ coincides with the stagnant region shown in [Figure](#)
[5\(b\)](#), which represents the region of the strong vertical flow at this vertical position as dis-
 cussed earlier. In the mid-depth plane, the SGF also influences the velocity field, where the
 355 length of the reverse flow becomes smaller (extends from $x/H = 0$ to $x/H = 0.98$) compared
 to the NGF case shown in [Figure 8\(a\)](#). Conversely, the SGF has no obvious effect on the
 velocity field in the near-surface plane, where $u_c/U_s = 0.0$ is located at $x/H \approx 1.52$. After-
 wards, u_c/U_s appears to increase with different rates in the downstream direction, where
 the highest rate occurs in the near-bed plane. Note that the curve of u_c/U_s in the near-bed
 360 plane is shown only to $x/H \approx 2.11$ because the velocity profiles in the wake become almost
 uniform after that. In the near-surface plane, u_c/U_s appears similar to the NGF case ($h_g/H =$
 0) shown in [Figure 8\(a\)](#).

The development of the central velocity u_c in the three horizontal planes for the LGF case ($h_g/H = 0.10$) is shown in [Figure 8\(c\)](#). Note that the position of the near-bed plane ($y/H = 0.10$) in this case matches the bottom edge of the bluff body ($h_g/H = 0.10$). This figure shows that the flow is forward (behind the bluff body) in the near-bed velocity field since the gap flow seems to have enough momentum to overcome the reverse flow. In addition, the length of the reverse flow region in the mid-depth and near-surface planes becomes smaller and extended only to $x/H \approx 0.89$ and 1.37 , respectively, compared to 0.98 and 1.52 for the SGF (see [Figure 8b](#)). At further downstream locations, the rate of increase is similar in the mid-depth and near-surface planes, while u_c , in the near-bed plane, increases with a slightly higher rate.

To highlight the effect of the gap flow, the development of the central velocity u_c/U_s for the three gap heights in the streamwise direction x/H is shown in [Figure 9\(a\)–\(c\)](#). [Figure 9\(a\)](#) visualises the effect of the gap flow on u_c/U_s in the near-bed plane. Compared to the NGF case, the forward central velocity u_c/U_s (just behind the bluff body) for the SGF case appears to be boosted by the gap flow as reflected by the larger magnitude and longer length. The following reverse flow becomes slightly smaller in magnitude and shifted downstream. Afterwards, the rate of increase in the SGF case, which is non-linear in both cases, is slightly larger than the NGF case. For the LGF case, the gap flow was more energetic and able to penetrate in the flow and eliminate formation of a reverse flow. Furthermore, u_c/U_s appears to grow non-linearly with a lower rate than the NGF and SGF cases in the range $1.23 < x/H < 2.08$, then with a higher rate at farther downstream locations ($x/H > 2.08$).

[Figure 9\(b\)](#) illustrates formation of a reverse flow (in all cases) in the mid-plane just behind the bluff body, where the length of the reverse flow region appears to decrease with increasing the gap flow. Further downstream, the magnitude of the central velocity u_c/U_s generally increases non-linearly in the downstream direction, where its magnitude increases with the increase of the gap height. However, the rate of increase in the three cases seems to be equal. This figure indicates that the wake flow in the mid-depth plane is directly influenced by the increase of the gap flow.

In the near-surface plane, the u_c/U_s curves for the NGF and SGF cases ($h_g/H = 0$ and 0.05) appear almost equal in the downstream direction as shown in [Figure 9\(c\)](#). However, u_c/U_s of the LGF case appears to be slightly larger in magnitude than the other cases as a result of the gap flow. Moreover, the length of the reverse flow region appears to be slightly smaller than the other cases. This indicates that the effect of the SGF ($h_g/H = 0.05$) on u_c is almost negligible in this plane, but the LGF ($h_g/H = 0.10$) has a mild effect on u_c/U_s in the near-surface plane, although the difference between the three cases seems to narrow at farther downstream locations.

5.5. Half-width of the wake

The half-width of the wake is defined as the transverse location z where the velocity defect $\Delta u (= u - U_s)$ equals half of the maximum velocity defect Δu_{\max} . In this paper, Δu_{\max} is defined as $(u_c - U_s)$, where U_s is the streamwise velocity at a corresponding vertical location without the body and u_c is the central velocity.

[Figure 10\(a\)–\(c\)](#) shows the variation of the wake half-width $W_{0.5}$ with the streamwise distance x extracted from the horizontal planes measured at vertical locations $y/H = 0.1$, 0.5 , and 0.8 , respectively. The half-width $W_{0.5}$ and the streamwise distance x are normalised by the width of the bluff body D and the water depth H , respectively. [Figure 10\(a\)](#) shows

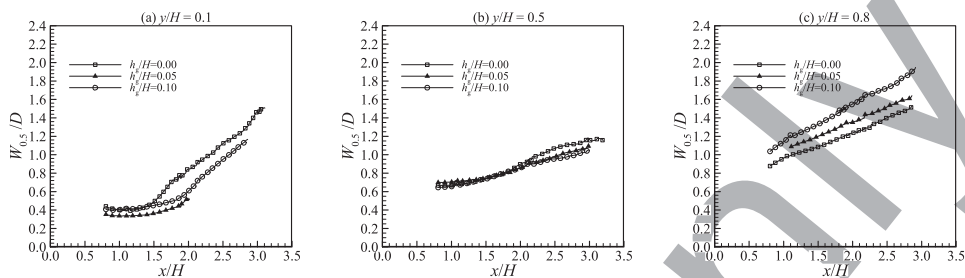


Figure 10. Development of the wake half-width $W_{0.5}$ in the streamwise direction x for the three gap heights h_g/H at (a) $y/H = 0.1$, (b) $y/H = 0.5$, and (c) $y/H = 0.8$. Both $W_{0.5}$ and x are normalised by the bluff-body width D and the water depth H , respectively.

that the half-width $W_{0.5}$ in the near-bed plane ($y/H = 0.1$) appears to be approximately constant in the beginning (in the three cases) until $x/H \approx 1.5$. Afterwards, the growth appears to increase somewhat linearly with a growth rate of 0.59 in the NGF case ($h_g/H = 0$), or increases gradually with a very small rate until $x/H \approx 1.90$ followed by a high linear growth of 0.65 as in the LGF case ($h_g/H = 0.10$). Note that the half width $W_{0.5}/D$ curve for the SGF case is shown only up to $x/H \approx 2.0$, because the velocity profiles are almost uniform after that (curve fitting is not possible).

The spread of the velocity profiles with the streamwise distance in the mid-depth plane ($y/H = 0.5$) shown in Figure 10(b) is different from Figure 10(a). The half-width $W_{0.5}/D$ curves appear to be almost identical in the three cases until $x/H \approx 2.0$, with a linear growth rate of approximately 0.20. Afterwards, the half width $W_{0.5}/D$ of the gap flow cases ($h_g/H = 0.05$ and 0.10) appears to grow with the same rate in the downstream direction, while the NGF case seems to be slightly higher.

The effect of the gap flow on the spread of the velocity profiles in the near-surface plane ($y/H = 0.8$) is shown in Figure 10(c). It is clear that the growth rate is linear in the three cases (in the range shown in the figure), and increases with increasing the gap flow. Specifically, the growth rates for $h_g/H = 0, 0.05$, and 0.10 are 0.30, 0.31, and 0.41, respectively.

In summary, the results illustrate clearly that there are significant differences in the growth rate in the three planes. The gap flow seems to have a limited effect on the growth rate in the mid-depth plane, but its effect is relatively large on the growth rate in the near-bed and near-surface planes. In the near-bed plane, the gap flow seems to delay the spread of the velocity profiles in the near-wake region, but they grow with a high rate at farther streamwise locations. In the near-surface plane, the gap flow causes an increase in the width of the velocity profiles with an approximately linear growth rate. Physically, the gap flow enhances the entrainment (inward flow) in the near-wake region in the near-bed plane as will be shown in Section 5.6. In addition, the gap flow also affects the transfer of the fluid throughout the water depth (by secondary currents) which could be the reason for the differences between the half-width of the profiles in the upper velocity fields.

5.6. Mean velocity profiles

Mean velocity profiles at selected downstream locations on the vertical (x, y) and horizontal (x, z) planes in the wake of the bluff body are presented in this section. Note that only some points on the velocity data are shown to avoid cluttering.

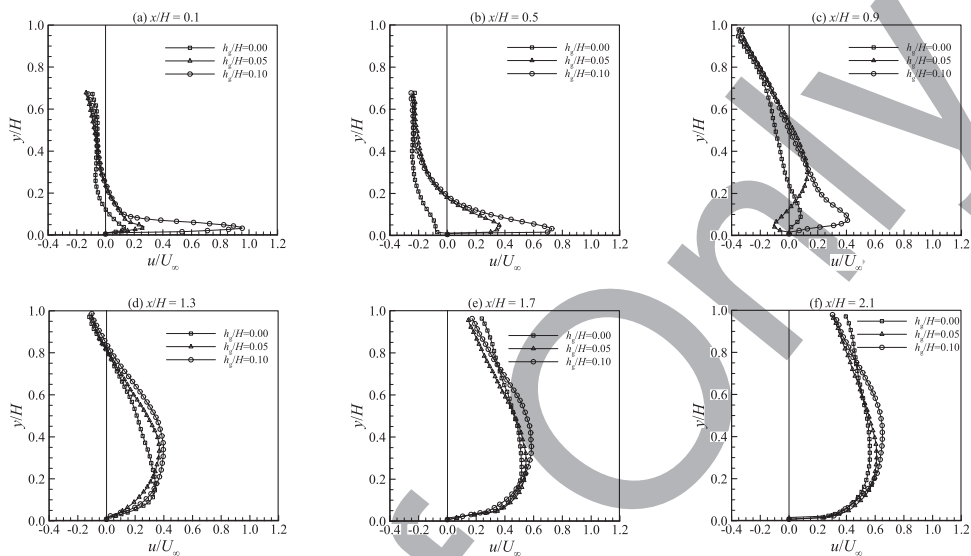


Figure 11. Mean streamwise u velocity profiles measured on the vertical mid-plane ($z/H = 0$) at different streamwise locations. The velocity u is normalised by U_∞ and location y by the water depth H .

5.6.1. Vertical plane profiles

440

The development of the streamwise u and transverse v velocity profiles in the streamwise direction for the three gap heights ($h_g/H = 0, 0.05$, and 0.10) is shown in Figures 11 and 12 measured along the vertical mid-plane ($z/H = 0$). All velocities (u and v) are normalised by the free-stream velocity U_∞ and are plotted against the vertical location y normalised by

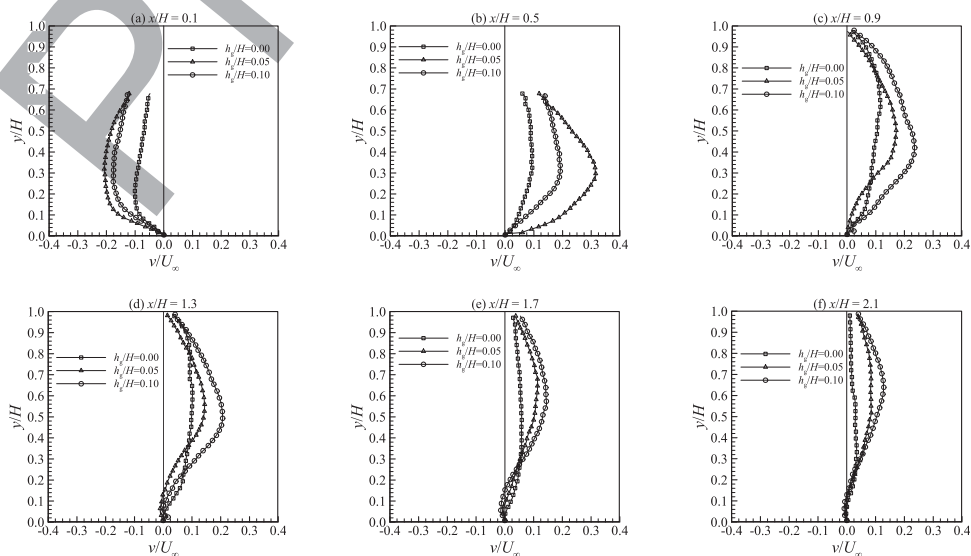


Figure 12. Mean vertical v velocity profiles measured on the vertical mid-plane ($z/H = 0$) at different streamwise locations. The velocity v is normalised by U_∞ and location y by the water depth H .

445 the water layer depth H . Since the origin of the coordinate system is at the bed, the lower solid boundary is at $y/H = 0$ and the free surface is at $y/H = 1.0$.

Figure 11(a)–(f) displays the effect of the gap flow on the streamwise velocity u profiles at different downstream locations measured on the vertical plane. It can be seen from Figure 11(a) that u appears positive in the NGF case ($h_g/H = 0$) for $y/H < 0.125$, and in the gap flow (SGF and LGF) cases ($h_g/H = 0.05$ and 0.10) for $y/H < 0.25$, while u is negative above these points. This is because these profiles represent a slice extracted from the CCW rotating recirculation zones formed in that region (see Figure 4). By comparing the velocity profiles at $x/H = 0.1$, the magnitude of the peak u velocity in the three profiles formed near the bed increases with increasing the gap height h_g . However, the peak velocity formed in the NGF case is because of the formation of a recirculation flow at this location (see Figure 4(a)). The peak values of u/U_∞ are 0.14, 0.27, and 0.95 for $h_g/H = 0, 0.05$, and 0.10 , respectively, located at $y/H = 0.03, 0.03$, and 0.04 .

At downstream location ($x/H = 0.5$), Figure 11(b) shows that the streamwise velocity u becomes negative (backward) throughout the FOV for $h_g/H = 0$. On the other hand, u , for the other two cases, varies from positive for $y/H < 0.19$ to negative above this point, where the u magnitude becomes larger throughout the captured water layer (excluding the peak value of the LGF case) compared to the corresponding profiles at $x/H = 0.1$. Interestingly, there is an increase in the peak velocity u/U_∞ for the SGF case ($h_g/H = 0.05$) from 0.27 to 0.37 m/s, while there is a decrease from 0.95 to 0.72 m/s for the LGF case ($h_g/H = 0.10$).

465 Further downstream ($x/H = 0.9$), Figure 11(c) shows that the streamwise velocity u appears to develop where u becomes positive near the bed and negative far from the wall for the NGF case ($h_g/H = 0$); u becomes negative near the bed and increases gradually to become positive and then negative again far from the wall for the SGF case; while, for the LGF case, u is still positive near the bed and negative far from the wall, but with larger u magnitudes compared to the corresponding profile at $x/H = 0.5$. The formation of a CW rotating recirculation zone (relatively small) at farther downstream locations for the $h_g/H = 0.05$ case (see Figure 4(b)) is the reason of the difference with the other profiles particularly for the LGF case. As discussed in Section 5.3, the CW recirculation zone is located close to the suspected transverse inward flow region near the bed, which seems to be fed from that region and then change its direction to flow upward to supply the backward and forward flows. The discrepancy between the velocity profiles shown in Figure 4(c) seems to decrease as the flow develops in the streamwise direction. At $x/H = 1.3$ (see Figure 11d), u becomes positive throughout most of the water depth with a mild peak which is shifted upward to $y/H = 0.32$ for SGF and LGF cases, and to $y/H = 0.16$ for the NGF case. Note that the small backward flow region (in all cases) near the free surface supplies the recirculation zone.

480 As the flow moves downstream, the three streamwise velocity u/U_∞ profiles at $x/H = 1.7$ appears to increase in magnitude throughout the water depth as shown in Figure 11(e). However, the rate of increase throughout the water depth is different in the three cases; e.g., the increase of u/U_∞ in the NGF case is larger in the upper half of the water depth ($y/H > 0.5$), while the increase for the SGF case is larger close to the wall ($y/H < 0.2$), compared to the other cases. The maximum magnitude of u/U_∞ is attained by the LGF case which is 0.59 located at $y/H = 0.35$, compared to 0.40 located at $y/H = 0.32$ at the streamwise location $x/H = 1.3$. This increase in the magnitude of the streamwise velocity u/U_∞ continues in the downstream direction with the same trend as shown in Figure 11(f). It shows that, at $x/H = 490$ 2.1, u/U_∞ still increases throughout the water depth although the increase in the upper half

is larger than the lower half. Since the rate of increase of u/U_∞ is higher in the upper half of the water depth, it is expected that u/U_∞ will finally become almost uniform throughout the water depth at downstream locations. This is confirmed in our results, but not shown because of space limitations.

The mean vertical velocity v/U_∞ profiles are shown in [Figure 12\(a\)–\(f\)](#). The velocity profile at $x/H = 0.1$, shown in [Figure 12\(a\)](#), illustrates that v is negative (downward) throughout the water depth captured in the FOV, where $|v|$ decreases gradually in the region $y/H < 0.1$ to reach zero at the bed. The largest magnitude of v is achieved by the SGF case, while the smallest $|v|$ is in the NGF flow case. Conversely, [Figure 12\(b\)](#) shows that v/U_∞ becomes positive (upward) throughout the captured water depth for all cases at $x/H = 0.5$, where the smallest and largest magnitudes of v/U_∞ are achieved by the NGF and SGF cases, respectively. The maximum magnitude of v/U_∞ for the SGF and LGF cases occurs at $y/H \approx 0.30$ ($v/U_\infty = 0.31$ and 0.19 , respectively); while for the SGF case, the v/U_∞ profile appears close to uniform. The downward and upward flows shown in [Figure 12\(a\)](#) and [12\(b\)](#), respectively, represent the flow at the peripheries of a CCW recirculation zones formed in all gap heights which explains the sign change of v/U_∞ (see [Figure 4](#)). However, the strength and size of these zones appear to vary with the gap flow, such that the largest strength is achieved by the SGF case. This increase in the strength in this case can be explained with the help of [Figure 4\(b\)](#) which illustrates that the gap flow is completely used to feed the recirculation zone.

At farther downstream location ($x/H = 0.9$), the velocity profiles shown in [Figure 12\(c\)](#) indicate that there is a significant change taken place in the gap flow cases ($h_g/H = 0.05$ and 0.10), while the change in the NGF case seems small. At this streamwise location, the velocity profiles still indicate an upward flow, but the magnitude of v/U_∞ becomes larger for the LGF case throughout the water layer compared to the SGF case. This is consistent with our previous observation that the upward flow in this case is fed by the gap flow. The peak value of v/U_∞ is approximately 0.17 and 0.24 located at $y/H \approx 0.49$ and 0.42 for SGF and LGF, respectively. As well, it can be observed that the rate of decrease of v/U_∞ is relatively large in the SGF case ($h_g/H = 0.05$) close to the bed ($y/H < 0.35$) when compared with the other profiles at this location and the previous location.

As the flow evolves downstream, [Figure 12\(d\)](#) shows that the mean vertical velocity v/U_∞ is still developing at $x/H = 1.3$ compared to the profiles shown earlier, where the velocity magnitudes decrease in the streamwise direction and the position of the peak velocity is shifted upward in the two gap flow cases. The position of these peak values is approximately coincident with the flow along the diagonal of the second FOVs shown in [Figure 4](#). [Figure 12\(d\)](#) also shows that the change in v/U_∞ in the NGF case is almost negligible except close to the free surface ($y/H > 0.8$) which appears to increase. The peak magnitude of v/U_∞ at this location is 0.14 and 0.21 located at $y/H \approx 0.53$ and 0.50 for SGF and LGF, respectively. It is interesting to see that, in addition to the SGF case, v/U_∞ for the LGF case also started decreasing with a relatively high rate close to the bed ($y/H < 0.35$) at this location. It is also interesting to see that v/U_∞ is downward near the bed in the SGF case, although its magnitude is very close to zero. Further downstream ($x/H = 1.7$), [Figure 12\(e\)](#) shows that the mean vertical velocity v continues to decrease in all cases throughout the water layer compared to [Figure 12\(d\)](#). The fastest decrease close to the bed occurs in the LGF case where v/U_∞ becomes negative (downward) in the range $y/H < 0.15$, while the decrease in the NGF case is relatively small in that region. However, v/U_∞ appears to increase in

the two gap flow cases close to the free surface, while v/U_∞ decreases in the NGF case with a relatively larger rate than the region near the bed. The velocity profile in the NGF case appears almost uniform throughout most of the water depth at this location where the magnitude is $v/U_\infty \approx 0.05$. This behaviour continues at $x/H = 2.1$ in all cases as shown in [Figure 12\(f\)](#). Specifically, v/U_∞ becomes almost zero near the bed ($y/H < 0.15$) in the three gap height cases. The reduction in v/U_∞ is expected to continue until v becomes almost zero at farther downstream locations.

The recirculation zones, formed just behind the bluff body in the gap and [NGF](#) cases on the vertical mid-plane ($z/H = 0$), appear to be stronger in the gap flow cases (particularly in the SGF case) compared to the NGF case. This behaviour is attributed to the gap flow which is completely used to boost the recirculation zone in the SGF case, while a portion of the gap flow is used to feed the recirculation zone in the LGF case and the other portion is directed downstream. Moreover, the results showed that there is a significant upward flow along the vertical mid-plane over most of the water depth. It seems that the upward flow is supplied by the inward transverse flow (entrainment) near the bed in the NGF and SGF cases and by the gap flow in the LGF case.

5.6.2. Horizontal plane profiles

The mean streamwise velocity u profiles on the horizontal plane are shown in [Figure 13](#). This figure consists of three columns which show the u profiles extracted from three horizontal planes: (i) the near-bed plane at $y/H = 0.1$, (ii) the mid-depth plane at $y/H = 0.5$, and (iii) the near-surface plane at $y/H = 0.8$. Each column consists of six plots (a, b, c, d, e, and f) which display the development of the u profiles in the streamwise direction x . Each plot presents the mean streamwise velocity u profiles for all three gap heights ($h_g/H = 0, 0.05, \text{ and } 0.10$). In this figure, the horizontal location z is normalised by the water depth H , and the velocity u is normalised by the mean streamwise velocity U_s ($U_s = 0.33, 0.42, \text{ and } 0.445$ m/s at the corresponding vertical location $y/H = 0.1, 0.5, \text{ and } 0.8$, respectively) of the channel flow without the body. Note that the edges of the bluff body in the horizontal plane are at $z/H = \pm 0.15$.

Plot (a) of [Figures 13\(i\)–\(iii\)](#) shows the u/U_s profiles at a streamwise location $x/H = 0.1$. The profiles are generally symmetrical about the vertical mid-plane ($z/H = 0$) and appear almost uniform in the core region ($|z/H| < 0.2$) where u/U_∞ is minimum, and increases with a very high rate for $|z/H| > 0.2$ to reach the maximum magnitude at $|z/H| \approx 0.25–0.30$, after which u/U_s gradually decreases. The three plots at this location ($x/H = 0.1$) represent three sections in a large CCW recirculation zone whose axis is perpendicular to the x – y plane and its horizontal span is approximately $0.4H$ ($\sim 1.33D$), where the flow is forward (positive) in the near-bed plane and backward (negative) in the upper planes with the strongest backward velocity occurring in near-surface plane. The gap flow appears to have boosted the forward and backward flows in the near-bed plane and mid-depth planes, respectively, whereas the magnitude of the backward velocity in the near-surface plane is not affected by the gap flow. However, the mean velocity u/U_s in the outer side ($|z/H| > 0.2$) appears to have increased by the gap flow in the near-bed and near-surface planes, whereas the increase in the mid-depth plane occurs only in the LGF case. The magnitude of u/U_s in the core region is approximately $0.13 \pm 0.03, -0.12 \pm 0.02, \text{ and } -0.25 \pm 0.01$ for the horizontal planes at $y/H = 0.1, 0.5, \text{ and } 0.8$, respectively, whereas the maximum u/U_s is $1.40 \pm 0.10, 1.15 \pm 0.10, \text{ and } 1.07 \pm 0.05$, respectively. At $x/H = 0.5$, plot (b) of [Figure 13\(i\)–\(iii\)](#)

shows that the shape of the u/U_s profiles in the near-bed and mid-depth planes resembles an inverted/flipped Gaussian profile, while the profiles in the near-surface plane are still uniform in the core region. This substantial difference in the shape (and magnitude) of the velocity profiles between the three horizontal planes refers to the three dimensionality of the 585

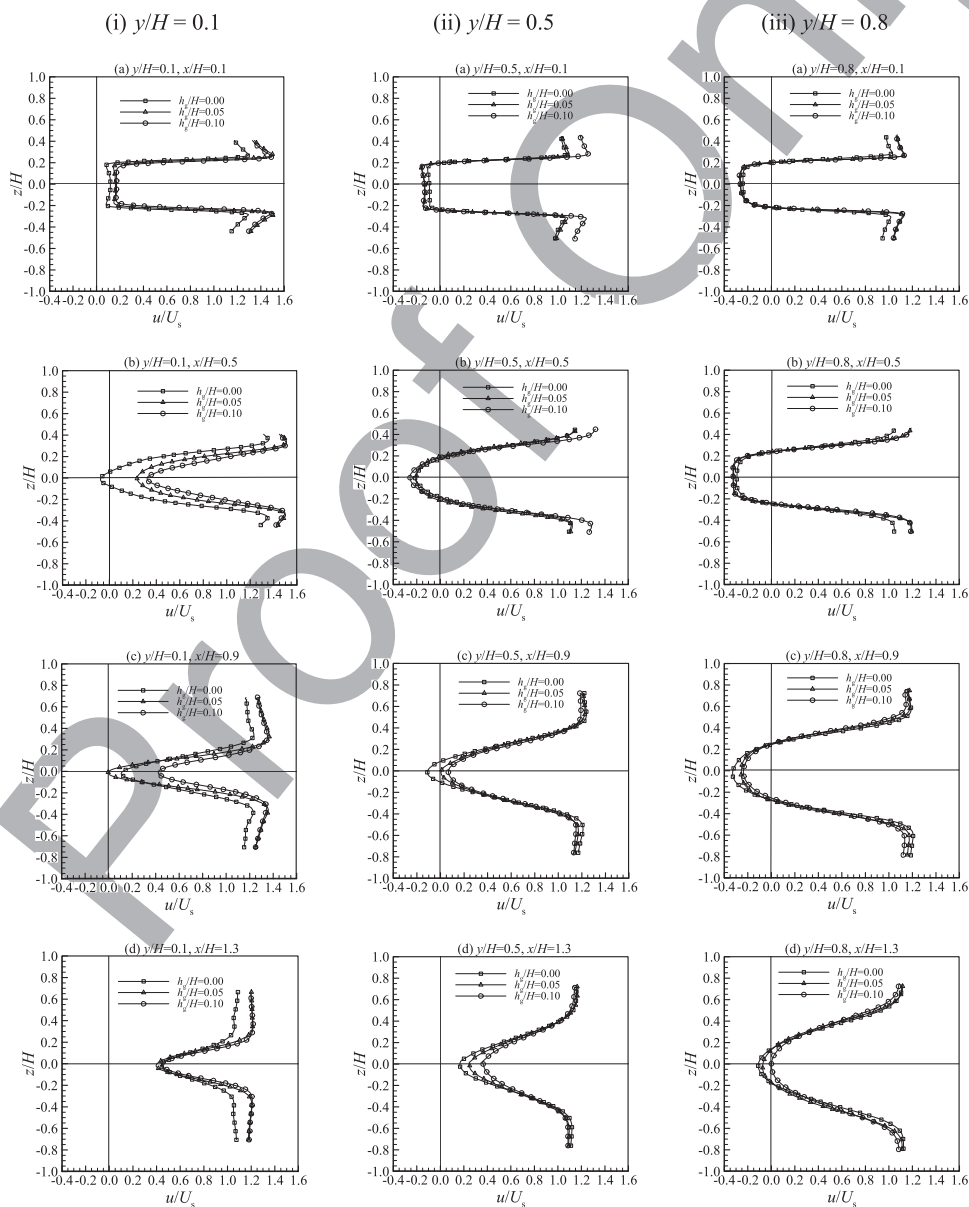


Figure 13. The mean streamwise velocity u profiles measured on the horizontal plane: (i) $y/H = 0.1$, (ii) $y/H = 0.5$, and (iii) $y/H = 0.8$. Each column (i, ii, and iii) consists of six plots (a, b, c, d, e, and f) which display the development of the u profiles in the streamwise direction x . Each plot presents u profiles for gap heights $h_g/H = 0, 0.05$, and 0.10 . The velocity u is normalized by U_s and the horizontal location z by the water depth H .

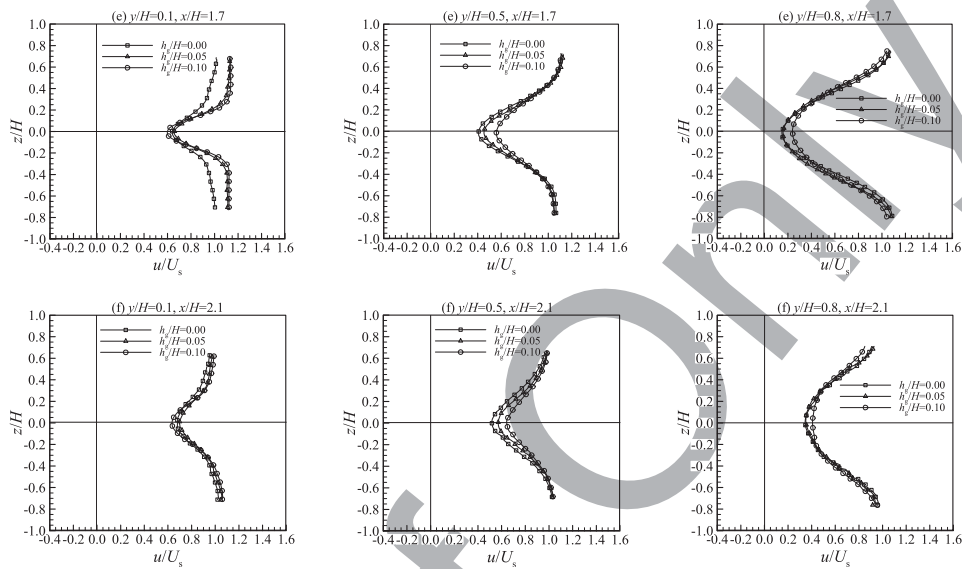


Figure 13. (Continued)

flow. The effect of the gap flow appears strong on u/U_s profiles in the near-bed plane ($y/H = 0.1$), but there is a slight effect on the mid-depth ($y/H = 0.5$) and near-surface ($y/H = 0.8$) velocity fields. Plot (b) of Figure 13(i) shows that u/U_s becomes negative (backward) in the NGF case of a relatively small magnitude in the range $|z/H| < 0.15$, which indicates that the recirculation zone is fed by flow that comes from the near-bed region in this case. In addition, the relatively large u/U_s magnitude at the sides of the gap flow cases is an indication of secondary currents which enhances the flow in that region as will be discussed later. At $x/H = 0.9$, the profiles shown in plot (c) of Figure 13(i)–(iii) illustrate an increase in u/U_s in the wake/core region (the wake shrink) in all planes, where the profiles in the near-bed plane is still different, while the profiles in the upper planes are reasonably coincident with a small deviation started appearing in the core region. It is interesting to see that u/U_s in the SGF case is the smallest in the core region ($u/U_s \approx 0$ at $z/H = 0$) and is not consistent with the trend of the profiles. By inspecting Figure 4(b), it is found that the streamwise position of the profile corresponds to the small CW recirculation zone (its axis is perpendicular to the x – z plane), where the velocity is almost stagnant in that region.

As the flow develops in the downstream direction, plots (d)–(f) of Figure 13(i)–(iii) show that u/U_s becomes equal for the three cases in the core region in the near-bed plane, while u/U_s of the gap flow cases appears larger in the outer case than the NGF case. On the other hand, the discrepancy between the profiles in the core region persists in the upper planes, although the profiles are matched in the outer region. At $x/H = 2.1$, the velocity profiles indicate vanishing of the effect of the gap flow at this location in this plane.

In summary, the above mean streamwise velocity u results show that the development of the near-bed velocity profiles is faster than the other planes. Furthermore, the gap flow generally causes an increase of u (in this plane) along the transverse direction in the streamwise range $x/H = 0.1$ – 0.9 . This increase continued in the streamwise direction to $x/H = 1.7$, but only at the sides of the velocity profiles. On the other hand, the effect of the gap flow

on u profiles, in the mid-depth and near-surface planes, is clear at the peripheries of the velocity profiles in the streamwise range $x/H = 0.1$ – 0.5 , and then in the core region (near the vertical mid-plane) in the rest of the presented velocity profiles.

The normalised mean transverse velocity w/U_s profiles extracted from the three planes 615 are shown in Figure 14(i)–(iii) at different streamwise locations. The arrangement of the plots is very similar to that in Figure 13. Similar to the u/U_s profiles, all figures show that

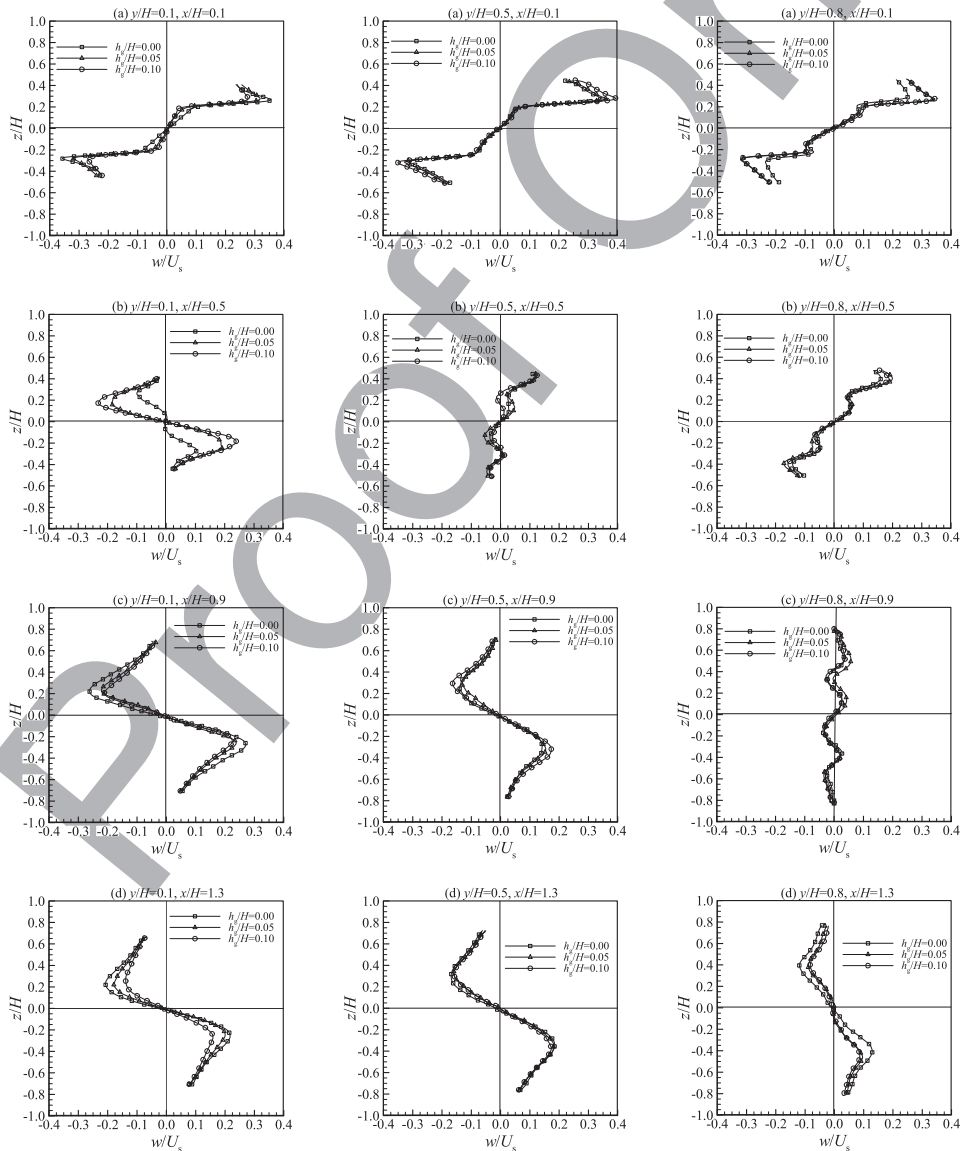


Figure 14. The mean transverse velocity w profiles measured on the horizontal plane: (i) $y/H = 0.1$, (ii) $y/H = 0.5$, and (iii) $y/H = 0.8$. Each column (i, ii, and iii) consists of six plots (a, b, c, d, e, and f) which display the development of the w profiles in the streamwise direction x . Each plot presents w profiles for gap heights $h_g/H = 0, 0.05$, and 0.10 . The velocity w is normalised by U_s and the horizontal location z by the water depth H .

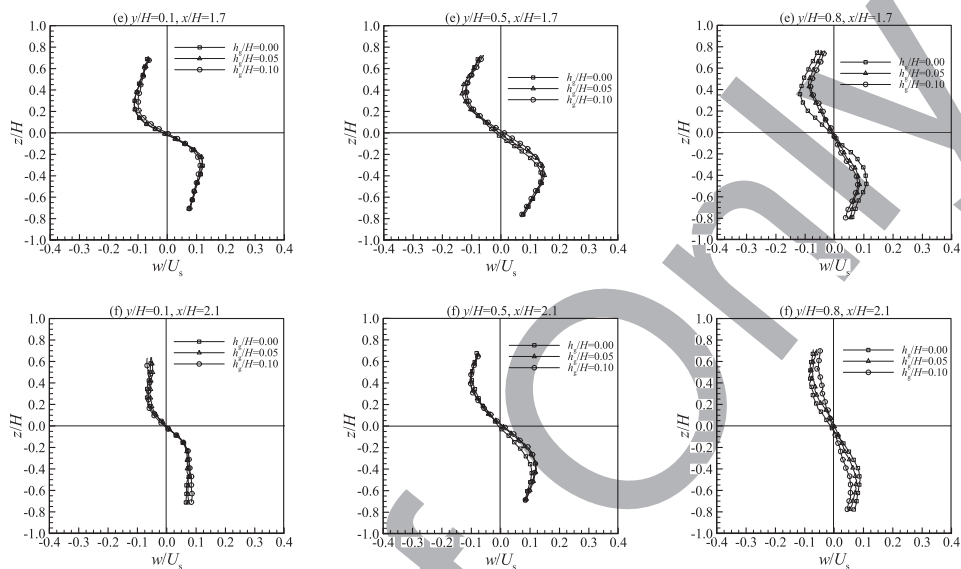


Figure 14. (Continued)

the transverse flow is symmetrical about the vertical mid-plane ($z/H = 0$) for all profiles and w/U_s is zero on the plane of symmetry.

620 Plot (a) of Figure 14(i)–(iii) illustrates that the transverse flow at $x/H = 0.1$ is outward from the vertical mid-plane for all gap height cases. It can also be seen that the transverse outward velocity increases linearly in the core region ($|z/H| < 0.2$), and then with a much higher rate in the region $0.2 < |z/H| < 0.3$. This outward flow at this location is a result of the diversion caused by the bluff body, which forces the working fluid to flow away from the bluff body. Even though the trend of the profiles in the three planes is similar, the near-bed velocity field appears to be more affected by the gap flow in the core and outer (peripheries) flow regions, whereas its effect in the upper planes is restricted to the outer flow region. The maximum magnitude of w/U_s for the gap flow cases ($h_g/H = 0.05$ and 0.10) is 0.32 , 0.37 , and 0.33 for the velocity fields at $y/H = 0.1$, 0.5 , and 0.8 , respectively. It is interesting to see
625 that the small drop of w/U_s in the near-surface plane at $|z/H| \approx 0.24$ corresponds to the edges of the wake region, where the flow changes its direction from backward flow in the core region to forward flow at the sides of the wake.

As the flow evolves in the streamwise direction, plots (b)–(f) in Figure 14(i)–(iii) illustrate a change in the transverse flow direction from outward flow to become finally inward flow at farther downstream locations. The results show that the transition from outward to inward flow in the near-bed plane took place in the region $0.1 < x/H < 0.5$. Similarly, the transition in the mid-depth plane took place at longer streamwise locations ($0.1 < x/H < 0.9$), while the transition in the near-surface plane took place at even longer distance ($0.1 < x/H < 1.3$). It can be concluded that the transition region occurs in a shorter distance as the horizontal velocity field gets closer to the bed. The w/U_s profiles in the near-bed plane, shown in plot (b) of Figure 14(i), display that the gap flow boosted the inward flow towards the vertical mid-plane, while the inward flow in the NGF case is weak with a velocity magnitude very close to zero in the range $|z/H| < 0.05$. The peaks' magnitude is $|w/U_s| \approx 0.10$,
635
640

0.19, and 0.23 for the $h_g/H = 0, 0.05,$ and 0.10 cases, respectively. At $x/H = 0.9$, plot (c) of Figure 14(i) illustrates that the flow is completely inward towards the vertical mid-plane ($z/H = 0$) for all gap height cases. However, the largest magnitude of w/U_s is reached by the NGF case ($|w/U_s| \approx 0.23 \pm 0.03$). As the flow develops in the streamwise direction, plots (d)–(f) of Figure 14(i) show that the magnitude of the inward flow appears to decrease and the effect of the gap flow diminishes as reflected by collapsing the three profiles into a single profile. In contrast to the near-bed plane, the velocity profiles in the mid-depth ($y/H = 0.5$) and near-surface ($y/H = 0.8$) planes, shown in plot (b) of Figure 14(ii) and 14(iii), indicate that the flow is still outward from the vertical mid-plane at $x/H = 0.5$. Further downstream, the flow becomes inward from $x/H = 0.9$ to 2.1 in the mid-depth plane and from $x/H = 1.3$ to 2.1 in the near-surface plane as shown in Figure 14(ii) and 14(iii), and the profiles are almost identical. The profiles in the transition region are characterised by a wavy shape with two peaks near the vertical mid-plane and two other peaks of larger magnitude in the outer region.

In summary, the effect of the gap flow is strong on the near-bed velocity field at locations $x/H < 1.3$, while its effect on the upper planes is restricted to the peripheries and on the near-wake region. Moreover, the possible scenario of the different flow directions in the three planes (see plots b and c) may be explained by the formation of a secondary flow in this region, where the fluid is inward in the near-bed plane, upward in the vertical mid-plane, and outward in the mid-depth and near-surface planes (see Section 5.3).

6. Conclusions

This experimental study describes the effect of the gap flow on a turbulent wake generated by flows past a vertical sharp-edged flat plate suspended in a shallow channel flow. Two different gap heights between the channel bed and the bottom edge of the bluff body ($h_g/H = 0.05$ and 0.10) were investigated, and compared to the NGF case ($h_g/H = 0$) which is considered as a reference case. Extensive PIV measurements were carried out throughout the developing wake region on both horizontal and vertical planes at a Reynolds number Re_H of 45,000. The conclusions may be summarised as follows.

- The wake flow is characterised by formation of recirculation zones on both horizontal and vertical planes. In the vertical plane, a CCW recirculation zone, whose axis is perpendicular to the (x, y) plane, was formed just behind the bluff body in the three gap heights ($h_g/H = 0, 0.05,$ and 0.10). The gap flow causes the centre of the recirculation zone to be slightly shifted upwards and to the right, and the shift increases with increasing the gap flow. On the other hand, the wake flow in the horizontal plane is characterised by formation of two recirculation zones of opposite rotational sense at the edges of the bluff body, whose axes are perpendicular to the (x, z) plane. The results revealed that the size of the wake varies in the three planes where the smallest wake is seen in the near-bed plane ($y/H = 0.1$), and it becomes even smaller with increasing the gap flow.
- The wake flow in the near-bed plane, just behind the bluff body, is characterised by a relatively small forward flow region, followed by a small reverse flow region, and then forward flow as in the NGF case. The weak gap flow (as in the SGF case) causes an increase in the length of the forward flow region and a slight decrease in the reverse flow region. However, the strong gap flow causes an elimination of the reverse flow

region as in the LGF case. On the other side, the wake flow in the mid-depth and near-surface planes is characterised by a relatively long reverse flow region which slightly decreases with increasing the gap flow.

- The flow is strongly three-dimensional and characterised by secondary flows. The results revealed a strong upward flow along the vertical mid-plane ($z/H = 0$) started near the bed and just behind the downstream boundary of the recirculation zone. The flow appears to be diverted upward along the diagonal of the second FOV in the streamwise range $0.7 < x/H < 1.7$ and up to the free surface ($y/H \approx 1.0$). As the upward flow progresses, a portion of it returns to supply the recirculation zone (reverse flow), and another portion flows in the downstream (forward) direction. Moreover, there is strong evidence that the upward flow was supplied by an inward transverse flow (entrainment) near the bed in the NGF and SGF cases. For the LGF case, the upward flow is supplied by the gap flow which penetrated downstream.
- When the gap flow is weak and does not have enough momentum to overcome the influence of the recirculation field whose axis is perpendicular to the vertical plane, it is completely engulfed by the recirculation zone and directed upwards as in the SGF case ($h_g/H = 0.05$), which explains the largest magnitude of the vertical velocity component v in that region. Conversely, if the gap flow is energetic enough, most of it will penetrate in the downstream direction and only a small portion flows upward to feed the recirculation zone as in the LGF case ($h_g/H = 0.10$).
- There are significant differences in the growth rate in the three planes. The gap flow seems to have a limited effect on the growth rate in the mid-depth plane, but the effect is relatively large on the growth rate in the near-bed and near-surface planes. In the near-bed plane, the gap flow enhances the entrainment (inward flow) in the near-wake region. In the near-surface plane, the growth rate is linear and appears smaller than the rate in the near-bed plane.

Acknowledgements



The support of the Natural Sciences and Engineering Research Council (NSERC) of Canada is gratefully acknowledged. The authors thank Arindam Singha for his role in carrying out some of the PIV measurements.

Disclosure statement

No potential conflict of interest was reported by the authors.

References

- [1] Burger E, Wille R. Periodic flow phenomena. *Ann Rev Fluid Mech.* 1972;4:313–340.
- [2] Wolanski E, Imberger J, Heron ML. Island wakes in shallow coastal water. *J Geophys Res.* 1984;89(6):10553–10569.
- [3] Chen D, Jirka GH. Experimental study of plane turbulent wakes in a shallow water layer. *Fluid Dyn Res.* 1995;16(1):11–41.
- [4] Lloyd PM, Stansby PK. Shallow-water flow around model conical islands of small side slope. Part I: surface piercing. *J Hydraul Eng.* 1997;123:1057–1067.
- [5] Balachandar R, Tachie MF, Chu VH. Concentration measurement in intermediate shallow wakes. *ASME J Fluids Eng.* 1999;121(1):34–43.

- [6] Nasif G, Barron RM, Balachandar R. DES evaluation of near-wake characteristics in a shallow flow. *J Fluids Struct.* 2014;45:153–163.
- [7] Akilli H, Rockwell D. Vortex formation from a cylinder in shallow water: flow structure and topology. *Phys Fluids.* 2002;14(9):2957–2967. 730
- [8] Singha A, Shinneeb A-M, Balachandar R. PIV-POD investigation of the wake of a sharp-edged flat bluff-body immersed in a shallow channel flow. *ASME J Fluids Eng.* 2009;131(2):021202–1.
- [9] Bosch G, Kappler M, Rodi W. Experiments on the flow past a square cylinder placed near a wall. *Exptl Thermal Fluid Sci.* 1996;13:292–305.
- [10] Bearman PW, Zdravkovich MM. Flow around a circular cylinder near a plane boundary. *J Fluid Mech.* 1978;89(1):33–47. 735
- [11] Price SJ, Sumner D, Smith JG, et al. Flow visualization around a circular cylinder near to a plane wall. *J Fluids Struct.* 2002;16(2):175–191.
- [12] Buresti G, Lanciotti A. Mean and fluctuating forces on a circular cylinder in cross-flow near a plane surface. *J Wind Eng Ind Aerodyn.* 1992;41:639–650. 740
- [13] Grass AJ, Raven PWJ, Stuart RJ, et al. The influence of boundary layer velocity gradients and bed proximity on vortex shedding from free spanning pipelines. *ASME J Energy Resour Technol.* 1984;106:70–78.
- [14] Taniguchi S, Miyakoshi K. Fluctuating fluid forces acting on a circular cylinder and interference with a plane wall. *Exp Fluids.* 1990;9:197–204. 745
- [15] Wang XK, Tan SK. Experimental investigation of the interaction between a plane wall jet and a parallel offset jet. *Exp Fluids.* 2007;42:551–562.
- [16] Taniguchi S, Miyakoshi K, Dohda S. Interference between plane wall and two-dimensional rectangular cylinder. *Trans Jpn Soc Mech Eng B.* 1983;49(447):2522–2529.
- [17] Durao DFG, Gouveia PST, Pereira JCF. Velocity characteristics of the flow around a square cross-section cylinder placed near a channel Wall. *Exp Fluids.* 1991;11:298–304. 750
- [18] Bailey SCC, Kopp GA, Martinuzzi RJ. Vortex shedding from a square cylinder near a wall. *J Turbul.* 2002;3(3):1–18.
- [19] Martinuzzi RJ, Bailey SCC, Kopp GA. Influence of a wall proximity on vortex shedding from a square cylinder. *Exp Fluids.* 2003;34:585–596. 755
- [20] Krampa-Morlu FN, Balachandar R. A study on the flow past a suspended bluff object in an open channel. *Can J Civil Eng.* 2001;28(4):547–554.
- [21] Krampa-Morlu FN, Balachandar R. Flow recovery in the wake of a suspended flat plate. *J Hyd Res.* 2007;45(2):270–278.
- [22] Ramamurthy AS, Ng CP. Effect of blockage on steady force coefficients. *ASCE J Eng Mech Div.* 1973;99:1050–1051. 760
- [23] Shinneeb A-M. Confinement effects in shallow water jets [PhD thesis]. Canada: University of Saskatchewan; 2006.
-  [24] Shinneeb A-M, Bugg JD, Balachandar R. Variable threshold outlier identification in PIV data. *Meas Sci Tech.* 2004;15:1722–1732. 765
- [25] Huang H, Dabiri D, Gharib M. On errors of digital particle image velocimetry. *Meas Sci Tech.* 1997;8:1427–1440.
- [26] Specialist Committee on Uncertainty Analysis of 25th ITTC. Uncertainty analysis – particle imaging velocimetry. Paper presented at: Intl Towing Tank Conference (7.5-01-03-03); 2008.
-  [27] Bugg JD, Rezkallah KS. An analysis of noise in PIV images. *J Vis.* 1998;1(2):217–226. 770
- [28] Clauser F. Turbulent boundary layers in adverse pressure gradient. *J Aerosp Sci.* 1954;21:91–108.
- [29] Balachandar R, Bhuiyan F. Higher-order moments of velocity fluctuations in an open channel flow with large bottom roughness. *J Hydraul Eng.* 2007;133:77–87.